SPECKLE DETECTION IN ULTRASOUND IMAGES USING FIRST ORDER STATISTICS

R. W. Prager, A. H. Gee,
G. M. Treece and L. Berman

CUED/F-INFENG/TR 415

July 2001

University of Cambridge
Department of Engineering
Trumpington Street
Cambridge CB2 1PZ
England

Email: rwp/ahg/gmt11 @eng.cam.ac.uk, lb@radiol.cam.ac.uk

Speckle Detection in Ultrasound Images using First Order Statistics

Richard Prager, Andrew Gee, Graham Treece and Laurence Berman*
University of Cambridge

Department of Engineering
Trumpington Street
Cambridge CB2 1PZ

*Department of Radiology
Addenbrooke's Hospital
Cambridge CB2 2QQ

Abstract

It is necessary to identify speckled regions in ultrasound images to control adaptive speckle suppression algorithms, for tissue characterisation, and to estimate the elevational separation of B-scans by speckle decorrelation. Previous authors have proposed classification techniques based on second order powers of the homodyned k-distribution, or lower order powers of the more limited k-distribution. In this paper we explore the speckle discrimination properties of statistics based on arbitrary powers of the ultrasound echo envelope signal using a combination of simulations and theoretical results from the homodyned k-distribution. We conclude that statistics based on powers less than one are surprisingly less effective than some higher powers. A simple discriminant function for speckle is evaluated quantitatively in simulation and qualitatively on sample B-scan images.

1 Introduction

Ultrasound B-scan images represent the back-scattering of an ultrasound beam from structures inside the body. There are two main types of scattering: diffuse scattering which leads to speckle in the image, and coherent scattering that creates clear light and dark features. Diffuse scattering arises when there are a large number of scatterers with random phase within the resolution cell of the ultrasound beam. Coherent scattering results when the scatterers in the resolution cell are in phase.

It is possible to parameterise regions of ultrasound B-scan images in terms of the number of scatterers in a resolution cell and the proportion of coherent, as opposed to diffuse, scattering. Let s^2 be the coherent signal energy and $2\sigma^2$ the diffuse signal energy. We use $k = s/\sigma$ as an indication of the proportion of coherent to diffuse reflectors, and μ as the effective number of scatterers per resolution cell.

If we can find k and μ for a patch in an ultrasound image, then we can use this information for speckle identification, to aid segmentation, and for tissue characterisation. Speckle identification is particularly useful as this is required for adaptive speckle suppression algorithms and for use in decorrelation algorithms to estimate the elevational distance between neighbouring B-scans.

Dutt and Greenleaf [2] describe a method for finding k and μ using the statistics of the ultrasound signal intensity, and a model based on the homodyned k-distribution. Data samples of over a thousand pixels are required to obtain stable statistics for such techniques.
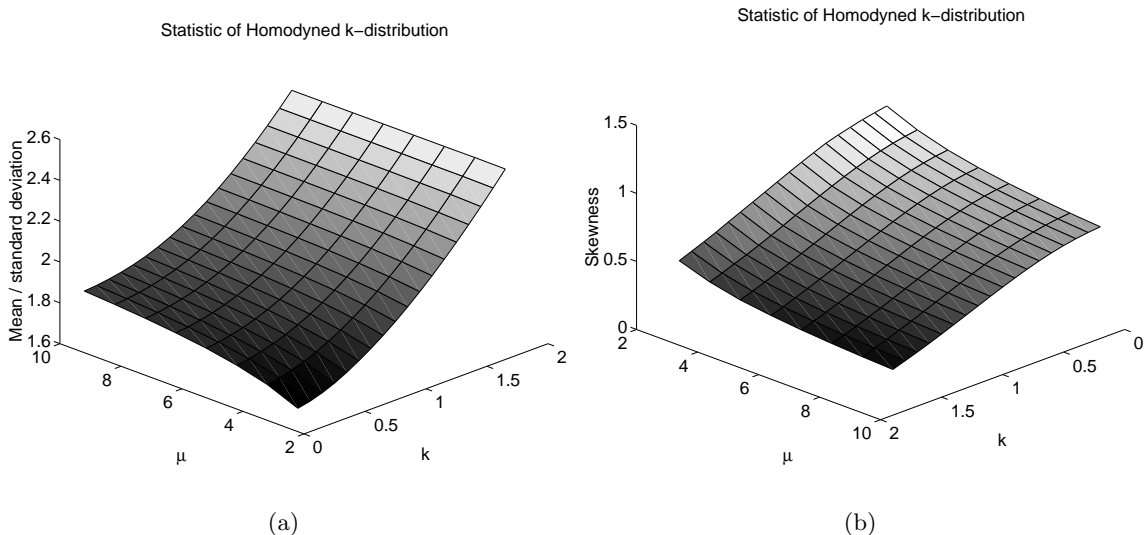
Figure 1: (a) shown the mean divided by the standard deviation of the homodyned k distribution for various values of μ, the number of scatterers per resolution cell, and k, the proportion of coherent to diffuse scattering. (b) shows the skewness of the homodyned k distribution for the same ranges of μ and k. Notice that both statistics depend strongly on k as well as μ. In data with varying k it would thus be impossible to infer μ based on the mean over the standard deviation alone.

There have therefore been attempts to use lower order statistics (eg. fractional order moments) in the hope that these measures will require smaller samples. Presumably because of the analytic inconvenience of the homodyned k-distribution, these approaches have been based on the k-distribution which is only a valid model in the absence of any coherent scattering [3, 5]. Preliminary experiments were performed in which the statistics used in [3] and [5] were calculated to a variety of powers in the range 0.25–2, both using the homodyned k-distribution and using simulations. In all cases the statistics had a strong dependency on k and a weak variation with μ, see for example Figure 1. In real B-scan images, where $k \neq 0$ cannot be ruled out, it is therefore impossible to use the k-distribution to find the effective number of scatterers, μ, without the results being severely corrupted by any coherent scattering present.

In this paper we extend Dutt and Greenleaf's original approach for inferring k and μ from sample statistics by exploring the performance of statistics that make use of data raised to different powers.

2   Choice of Statistic for Speckle Discrimination

To find k and μ we need two statistics. Having found k and μ we can then label as speckle patches with high μ and low k. Following [2] we choose the ratio of the mean to the standard deviation, and skewness. Based on [3, 5] we calculate these statistics on arbitrary powers v

of the data values A.

$$R \; = \; \frac{\text{mean}}{\text{standard deviation}} = \frac{\langle A^v \rangle}{\sqrt{\langle A^{2v} \rangle - \langle A^v \rangle^2}} = \frac{1}{\sqrt{\langle J^{2v} \rangle - 1}} \tag{1}$$

$$S \; = \; \text{skewness} = \frac{\langle (A^v - \langle A^v \rangle)^3 \rangle}{(\langle A^{2v} \rangle - \langle A^v \rangle^2)^{\frac{3}{2}}} = \frac{\langle J^{3v} \rangle - 3 \langle J^{2v} \rangle + 2}{(\langle J^{2v} \rangle - 1)^{\frac{3}{2}}} \tag{2}$$

$$\text{where } \langle J^v \rangle = \langle A^v \rangle / \langle A \rangle^v$$

Based on the results in [3, 5], we are expecting values of v less than one to perform well. We therefore perform simulations to select the value of v for which R and S have maximum variation to discriminate speckle from non-speckle, and the lowest possible noise variance.

To generate a simulated sample, the sum of μ vectors of length $\sqrt{2/\mu}$ and random phase is added to a single vector with (arbitrarily) zero phase and length k. The amplitude of the total provides a single sample A, with $\sigma = 1$. For the simulations, we use ($k = 0$, $\mu = 50$) to represent speckle, and three combinations, ($k = 1$, $\mu = 50$), ($k = 0$, $\mu = 2$), and ($k = 1$, $\mu = 2$) to represent various types of non-speckle. Five thousand sets of 500 random samples were generated for each of the four combinations of k and μ. For each value of v, the standard deviation among the R values for the four (k,μ) combinations was divided by the standard deviation among the 5000 different times the R statistic was calculated. This gave a measure of the meaningful variation in R divided by the noise in measuring R for each of the (k,μ) combinations. This measure is shown, as a function of v, in Figure 2(a). The same measure is shown for S in Figure 2(b).

Figure 2(c) shows the minimum value of all of the graphs in Figures 2(a) and 2(b) for each value of v. Surprisingly, values of v less than 1 are not necessarily the most effective for speckle discrimination. The values close to $v = 1$ appear unattractive, and values close to $v = 2$ seem, on the basis of this simulation, to perform well. Using $v = 2$ results in Dutt & Greenleaf's algorithm for speckle detection [2] which has an efficient closed form solution derived in [6].
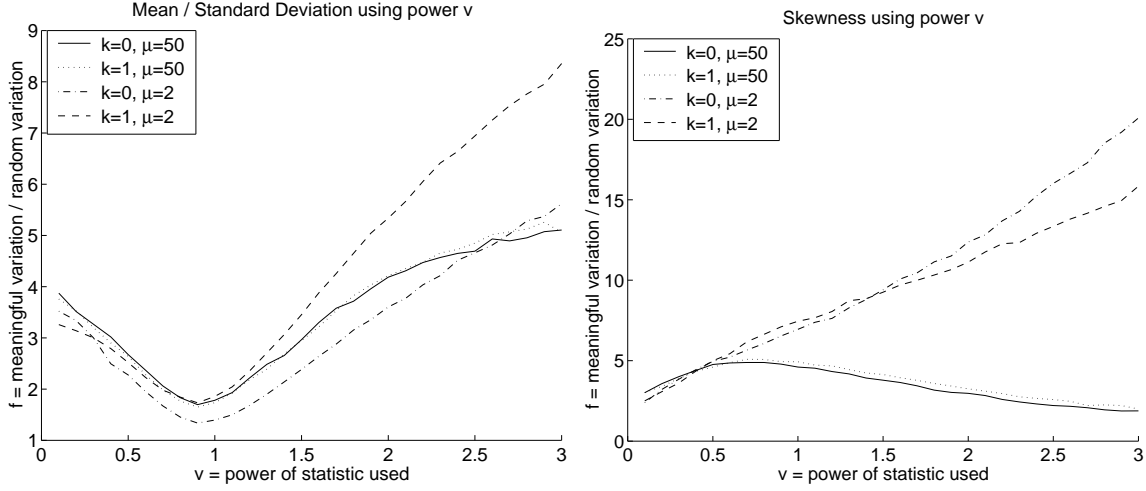
For the next two sections of this report we take the peak of the graph in Figure 2(c) and choose $v = 1.8$. At the end of the report we will explore the performance of a simpler approach with $v = 2$. Using Equations 1 and 2 together with this value of v, we have complete definitions of the statistics, R and S, to be used.

3 Discriminant Function for Speckle

We now have to design a discriminant function in (R, S) space to separate speckle from non-speckle based on the B-scan echo envelope amplitude. We do this by exploring the regions of (R, S) space occupied by speckle, first using the homodyned k-distribution, and then with simulations.
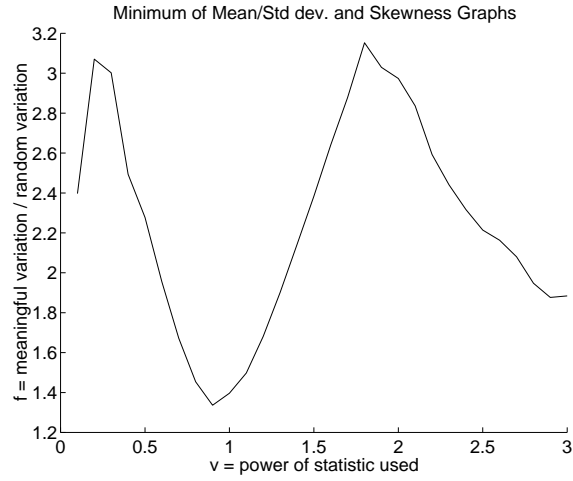
The homodyned k-distribution models the amplitude signal from μ weak scatterers with $\langle A^2 \rangle = 2\sigma^2$, and coherent scattering amplitude s [4]. The moments can be calculated by numerical integration of (corrected) Equation B.15 in [1].

$$\langle A^v \rangle = \int_0^\infty \left(\frac{2\sigma^2}{\mu} \right)^{\frac{v}{2}} \frac{\Gamma \left(1 + \frac{v}{2} \right)}{\Gamma(\mu)} x^{\left(\frac{v}{2} + \mu - 1 \right)} e^{-x} {}_1F_1 \left(\frac{-v}{2}; 1; \frac{-\mu s^2}{2\sigma^2 x} \right) dx \tag{3}$$

Figure 2: In (a), the statistic R (see Equation 1) is computed 5000 times on samples of size 500 for the four cases shown in the legend. The value f plotted is the standard deviation between the four cases, divided by the standard deviation within each case. Each line is labelled with the case used in the denominator. k is the ratio of coherent to diffuse scattering. μ is the effective number of scatterers per resolution cell. v is the power used in calculating the statistic R. (b) shows the same graphs for the statistic S (see Equation 2). (c) shows the minimum of the eight graphs in (a) and (b) for each value of v.
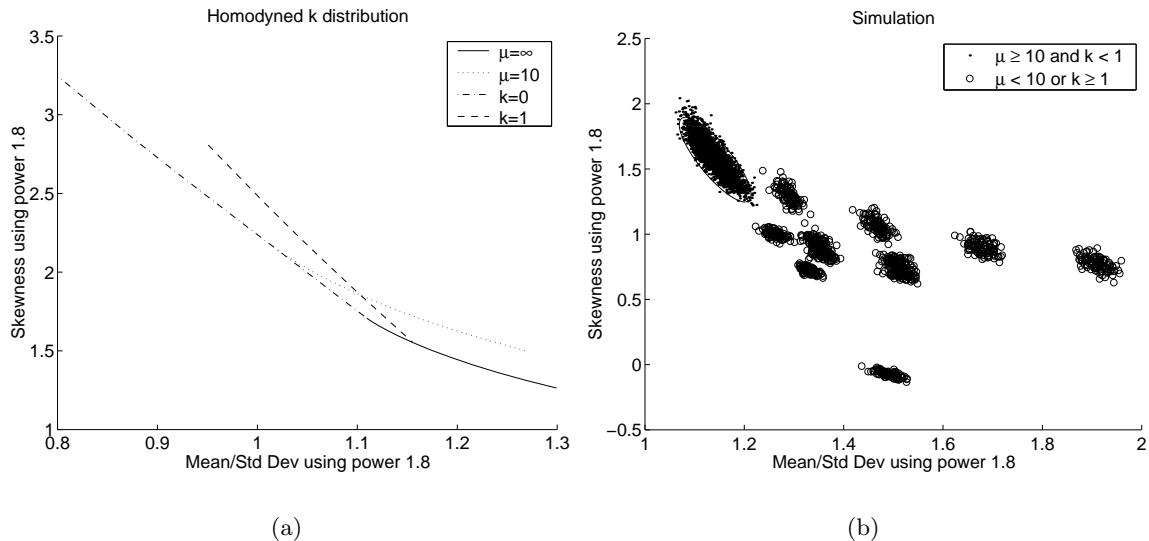
Figure 3: (a) shows the statistics R and S (see Equations 1 and 2), computed from the moments of the homodyned k-distribution to the power of 1.8. The (R, S) values inside the triangular shaped region correspond to speckle. (b) shows the same statistics computed on samples of 4000 simulated speckle values as described in Section 3. The dots correspond to speckle and the circles to non-speckle. The ellipse drawn around the group of dots is the chosen discriminant function. k is the ratio of coherent to diffuse scattering. μ is the effective number of scatterers per resolution cell.

For more details on distributions for modelling speckle see Appendix A. Numerical integration of the confluent hypergeometric function $_1F_1$ was performed using the Maple (Waterloo Maple Software) and Matlab (The Mathworks Inc.) programs to produce the graph in Figure 3(a). In theory, speckle with $\mu > 10$ and $k < 1$ corresponds to the triangular area between the lines.

For the simulations, data was generated as in the previous section, but this time using samples of size 4000 rather than 500. Figure 3(b) shows (R, S) space with a variety of samples based on $\mu \geq 10, k < 1$ plotted as dots and samples with $\mu < 10, k \geq 1$ plotted as circles. Fully developed speckle with $k = 0$ and $\mu > 50$ comes out in the same place for the theory and the simulations. The shape of the area corresponding to speckle statistics is however different, particularly for low values of μ. This is because of the difference between the way μ is used to determine the effective number of scatterers in the homodyned k-distribution and the direct use of μ to determine the number of weak scatterer vectors in the simulation.

Based on these initial experiments, an elliptical discriminant function was chosen for systematic evaluation by simulation. The orientation of the ellipse was determined by eigenvector analysis of the covariance matrix of an (arbitrary) sample of points corresponding to various kinds of speckle. The size of the ellipse was determined manually. The result is shown in Figure 3(b). The systematic evaluation was performed as follows. For all combinations of $0 < k < 3$ and $2 < \mu < 50$ a hundred values of R and S were generated using samples of
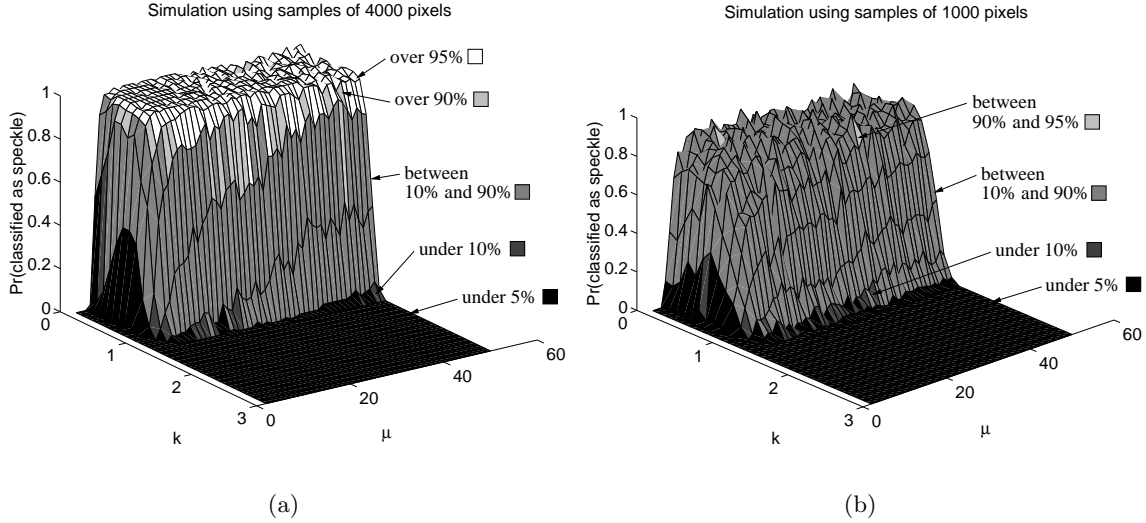
5

Figure 4: (a) shows the result of a simulation to evaluate the elliptical discriminant function for speckle selection. 100 sets of 4000 data points were evaluated for each combination of k, the ratio of coherent to diffuse scattering, and μ, the effective number of scatterers per resolution cell. The probability of each (k, μ) combination being classified as speckle was estimated. The diagram shows clear thresholds at $k = 1.1$ and $\mu = 6$. (b) shows the same diagram, only using samples of 1000 rather than 4000 data values. Notice that there are no probabilities above 95%, and the general performance is degraded.

size 4000. The 100 values were used to estimate the probability that simulated data with each combination of k and μ parameters would fall inside the ellipse and thus be classified as speckle. These probabilities are shown in Figure 4(a). The figure shows pleasingly clear discriminant boundaries at $k = 1.1$ and $\mu = 6$, which are plausible values for a simple speckle detector.

The experiment was repeated using samples of 1000 rather than 4000 data values. The results are shown in Figure 4(b). Note the degradation in performance. Few combinations of μ and k that we would expect to correspond to speckle result in a 90% probability of correct classification, and none of these are over 95%.

4   Evaluation on B-scans

Ultrasound images were decompressed to yield the approximate echo envelope amplitude using the technique described in [6], adapted to use R and S (with $v = 1.8$) as the target statistics[1]. The mean values for R and S for hand labelled speckle in the resulting images were then used as the centre point of the elliptical discriminant function. The rule for speckle detection was thus very simple and fast to implement: calculate R and S and if the values lie in the ellipse call the patch 'speckle'. Based on the results of the previous section we should aim for
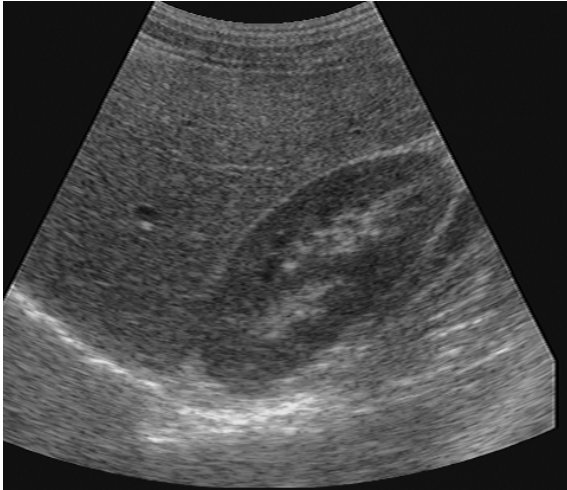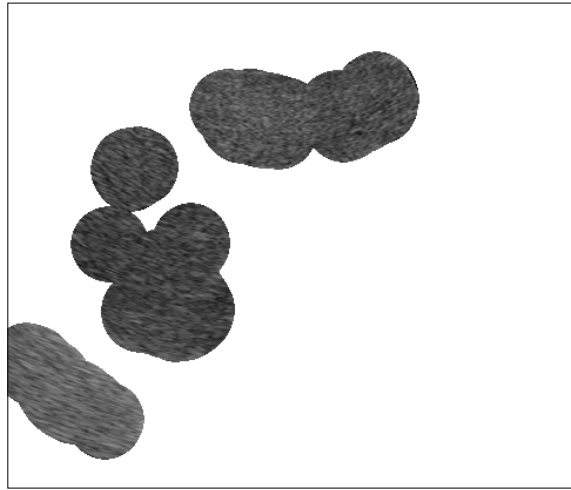
---

[1]See Section 5.1 for further description of this algorithm
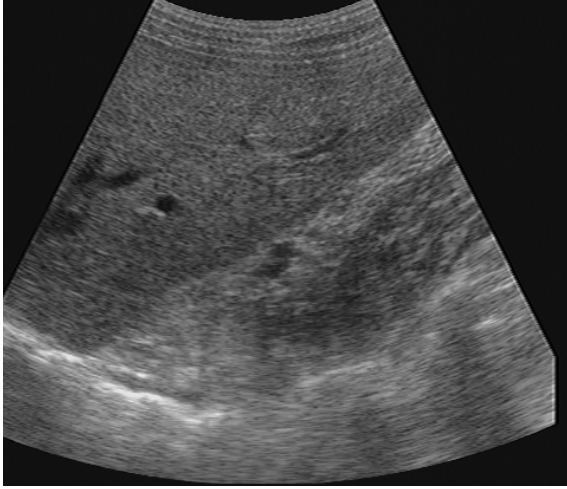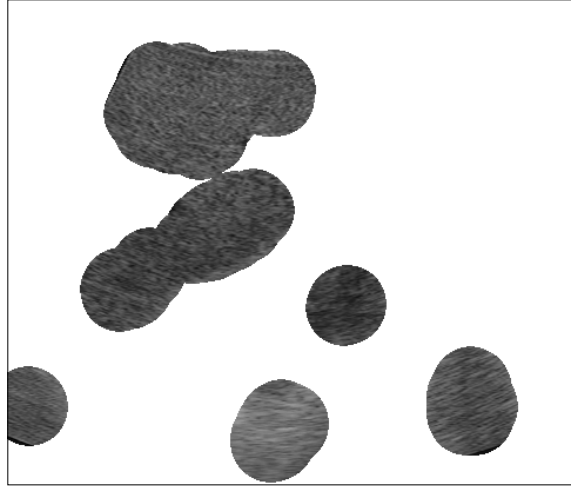
Figure 5: (a) shows an image from an ultrasound scan of a liver, and (b) shows the regions classified as speckle in this image using the elliptical discriminant function in (R, S) space from Figure 3(b). (c) and (d) show the same thing for the 164th image of the same scan. This includes a kidney as well as the liver.
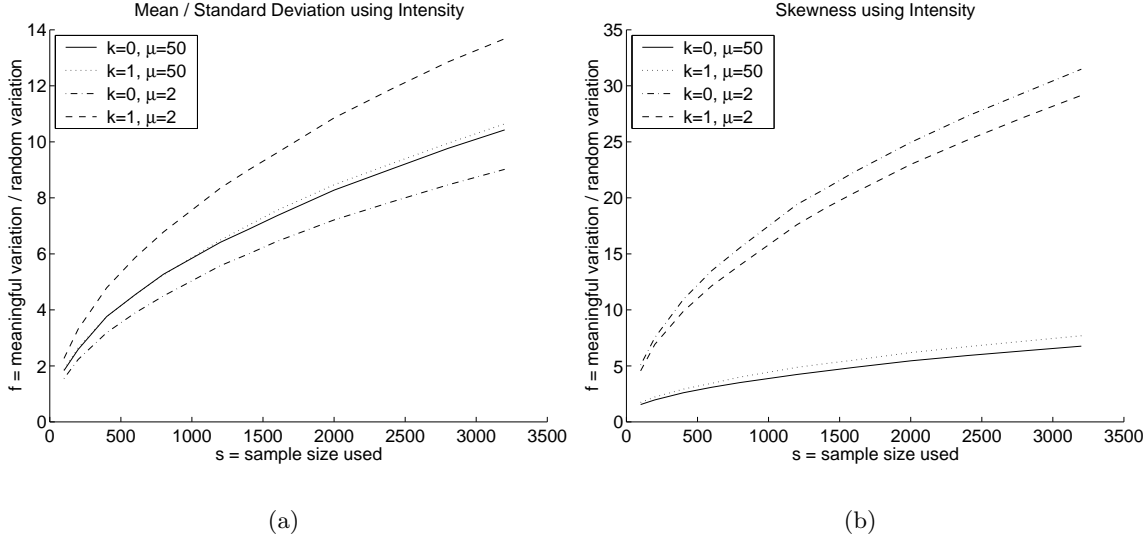
Figure 6: The effect of sample size on two statistics R = mean / standard deviation, and S = skewness. In (a), the statistic R (see Equation 1, $v = 2$ to use the intensity signal) is computed 5000 times on different sizes of sample for the four cases shown in the legend. The value f plotted is the standard deviation between the four cases, divided by the standard deviation within each case. Each line is labelled with the case used in the denominator. k is the ratio of coherent to diffuse scattering. μ is the effective number of scatterers per resolution cell. s is the number of samples used in calculating the statistic R. (b) shows the same graphs for the statistic S (see Equation 2).

a sample size close to 4000 to use for estimating the R and S statistics. We choose circular patches of radius of 32.2 pixels containing 3249 samples.

Figures 5(a) shows an image from an ultrasound scan of a liver. Figure 5(b) shows the patches in this B-scan classified as speckle by the algorithm above. The technique appears to be successful at picking patches with a relatively uniform speckled appearance. It appears to work best using a large sample size and this limits its ability to perform fine-grained analysis.

5   Efficient Implementation

We have presented a speckle segmentation technique that appears to work well using large samples of amplitude data raised to the power of 1.8. The goal in this section is to simplify the algorithm and run it on smaller samples of data so as to obtain better resolution. The reliability will be reduced, but the resulting simple strategy may be more useful.

Previous work in the field [2, 6] has used the envelope intensity signal which is equivalent to $v = 2$ in Equations 1 and 2. It is also more likely that the intensity signal will be conveniently available from ultrasound machines than the amplitude to the power of 1.8. In this section, we therefore reformulate the speckle segmentation algorithm for $v = 2$ rather than $v = 1.8$.
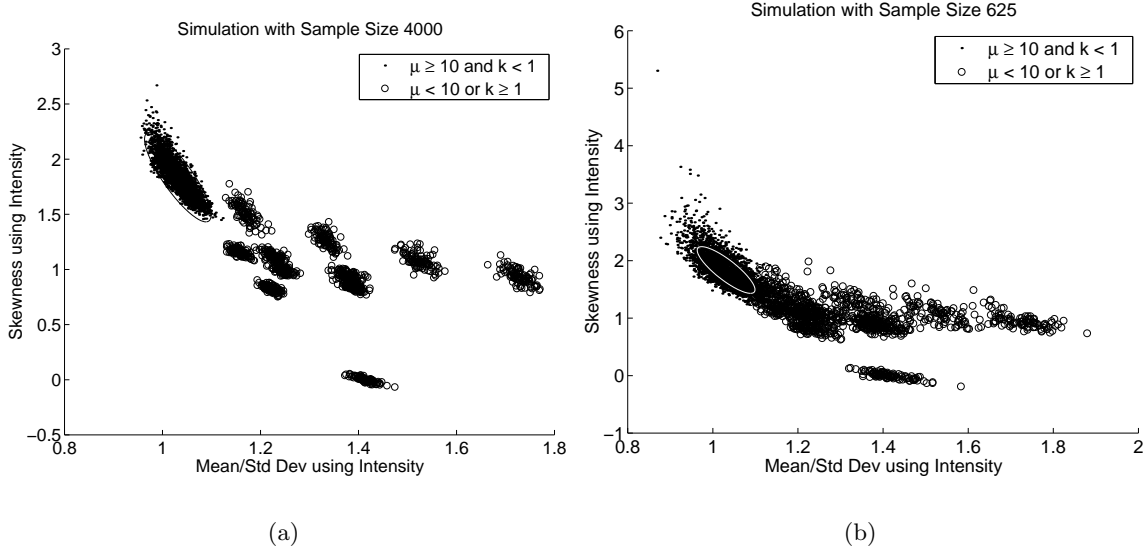
Figure 7: (a) shows the statistics R and S (see Equations 1 and 2) computed on samples of 4000 simulated data values (generated as before in Section 3), only this time using $v = 2$. The dots correspond to speckle and the circles to non-speckle. The ellipse drawn around the group of dots is the chosen discriminant function. k is the ratio of coherent to diffuse scattering. μ is the effective number of scatterers per resolution cell. (b) shows the same statistics, only this time calculated on samples of size 625. The discriminant function devised using (a) is also shown in (b).

Next we wish to reduce the size of samples used to compute R and S. Figure 6 shows the effect of sample size on the discriminant power of the two statistics individually. The higher each graph, the greater the variation between the different types of simulated images, and the lower the measurement noise in the statistic. Notice that the worst results are obtained for skewness on images with a large number of diffuse scatterers. In these cases measurement noise is particularly high.

As a design compromise we choose a sample size of 625. The simulations from Section 3 were repeated using the intensity signal and sample sizes of both 4000 and 625. Figure 7(a) shows the results with the samples of 4000. This figure was used to design the discriminant function by fitting an ellipse around the cloud of speckle data points. The chosen ellipse is centred at $R = 1.031$, $S = 1.837$ with a semi-major axis of 0.41 and a semi-minor axis of 0.036. The angle between the semi-major axis and the positive R axis is 81.9 degrees. It is also shown in white on Figure 7(b). As one would expect, in (b) the distinction between the different categories of simulated image is much less clear because of the smaller sample size.

The elliptical discriminant function designed using Figure 7(a) is evaluated by means of exhaustive simulation. The results are presented in Figure 8. The results are very much as expected. The simulation with samples of 4000 produces excellent results although, compared to Figure 4, it is noticeable that a smaller proportion of the simulated speckle is classified correctly more than 95% of the time. Considering the region of the histogram for $\mu \geq 10$ and
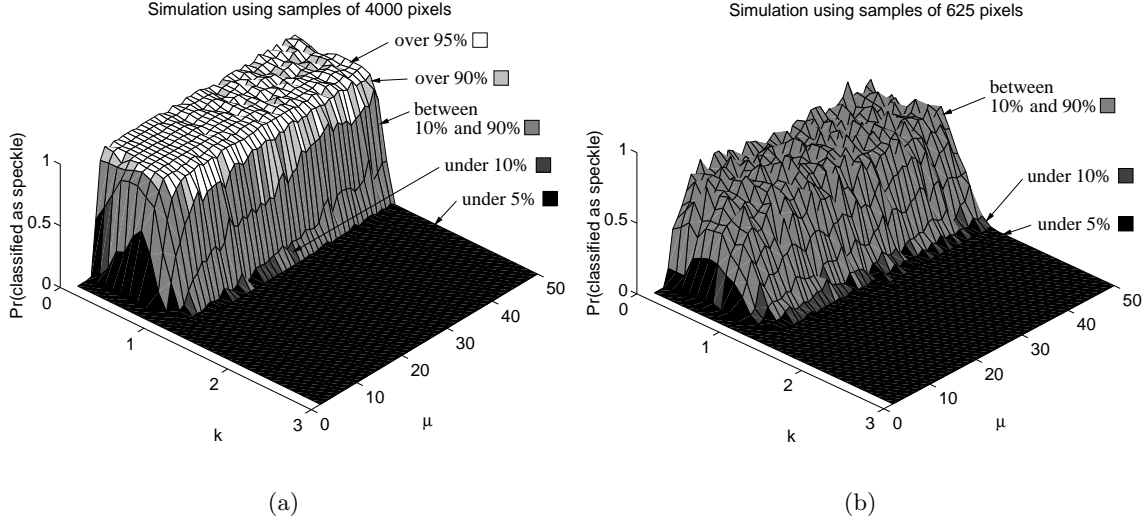
Figure 8: (a) shows the result of a simulation to evaluate the elliptical discriminant function for speckle selection using intensity data ($v = 2$). 100 sets of 4000 data points were evaluated for each combination of k, the ratio of coherent to diffuse scattering, and μ, the effective number of scatterers per resolution cell. The probability of each (k, μ) combination being classified as speckle was estimated. The diagram shows clear thresholds at $k = 1.2$ and $\mu = 6$. (b) shows the same diagram, using samples of 625 rather than 4000 data values. Notice that there are no probabilities above 90%, and the general performance is degraded.

$k \leq 1$, 91% of the points in Figure 4(a) are above 95%, whereas the same figure for Figure 8(a) is only 84%. This could be because the cloud of points in Figure 7 is less elliptical in shape than that in Figure 3(b). The performance of the classifier based on samples of 625 is worse, but a clear boundary around $k = 1.3$ and $\mu = 5$ still exists.

5.1 The Complete Algorithm

We now present the complete algorithm, and show the qualitative results when it is used to extract regions from a number of different ultrasound image sequences. First the B-scan images must be decompressed to recover an approximation to the envelope intensity data. A modified version of the algorithm introduced in [6] is used. This is described below for completeness. The goal is to find an appropriate value of D to use in

$$\text{Intensity} = \exp(\text{Pixel value}/D)$$

to map pixel values onto intensity values. Using this strategy we obtain intensity directly, rather than amplitude. We must therefore use $v = 1$ rather than $v = 2$ in Equations 1 and 2 to obtain R and S based on the second power of the amplitude. (It is simple to show that if D_A decompresses to amplitude and D_I decompresses to intensity, then $D_A = 2D_I$).

1. Choose an initial value for D. (We use 40; the algorithm is not particularly sensitive to the starting value.)

2. Manually label a number of patches of speckle in some of the B-scan images.

3. Invert the compression mapping for the data in the patches of known speckle using

$$\text{Intensity} = \exp(\text{Pixel value}/D)$$

4. Compute the statistics R and S on each patch of the estimated intensity data.

5. Calculate an error vector with two components for each patch. If an (R, S) point lies in the ellipse defined in Figure 7 then the corresponding two components of the error vector are taken as zero. If the (R, S) point lies outside the ellipse, the corresponding two components of the error vector are taken as the errors in R and S compared to the centre point of the ellipse $(1.031, 1.837)$.

6. If the sum squared magnitude of the error vector is small compared to the machine precision, or the search has converged to a (potentially local) minimum of this error function: finish.

7. Use an optimisation algorithm (*e.g.* Levenberg Marquart) to estimate a value of D that reduces the sum squared magnitude of the error vector. Continue from step 3.

The results in this report are based on about 4 square patches, 25×25 pixels, of hand labelled speckle across 10 or more images. This gave a total of at least 40 patches, each with 625 samples.

The decompression process provides three pieces of information: the value of D, and the average values of R and S across all the patches of manually labelled speckle. These average values are used to locate the centre point of the elliptical speckle discriminant function for each set of data. The orientation and size of the ellipse remains fixed as defined above.

Speckle detection is now very easy. Work out R and S on any patch of the intensity image and if the point lies in the discriminant ellipse classify the patch as speckle. If it lies outside the ellipse classify it as non-speckle. For the results in this report, patches of radius 14.1 pixels were used. This gave a sample size of 621.

The results presented in Figures 9 and 10 are all based on ultrasound images taken from sweeps of many images recorded sequentially. Neither of the figures contain any of the B-scan images in which the speckle was labelled manually for the decompression algorithm. These were taken at other stages in the same sweep, and each sweep was decompressed using an appropriate value of D. Figure 9(a) shows a scan through a liver and kidney using a 3.5 MHz probe on a Toshiba Powervision, Figure 9(b) shown the speckle detected in this image. Figures 9(c) and (d) show the same thing for a scan of a 16 week fetus using the same scanner. Figures 10(a) and (b) show the carotid artery and were obtained using a Dynamic Imaging Diasus scanner with a 5–10 MHz probe. Figures 10(c) and (d) show a thyroid scanned with a 7 MHz probe on a Toshiba Powervision.

Given the simplifications that have been made to the algorithm and the small sample size used, the results appear good. Notice how Figure 9(b) shows the speckle inside the outer rim of the kidney, but omits the coherent scattering in the centre of the organ and at its boundary. A similar effect can can be observed in Figure 9(d) where the speckle inside the

(a)   (b)

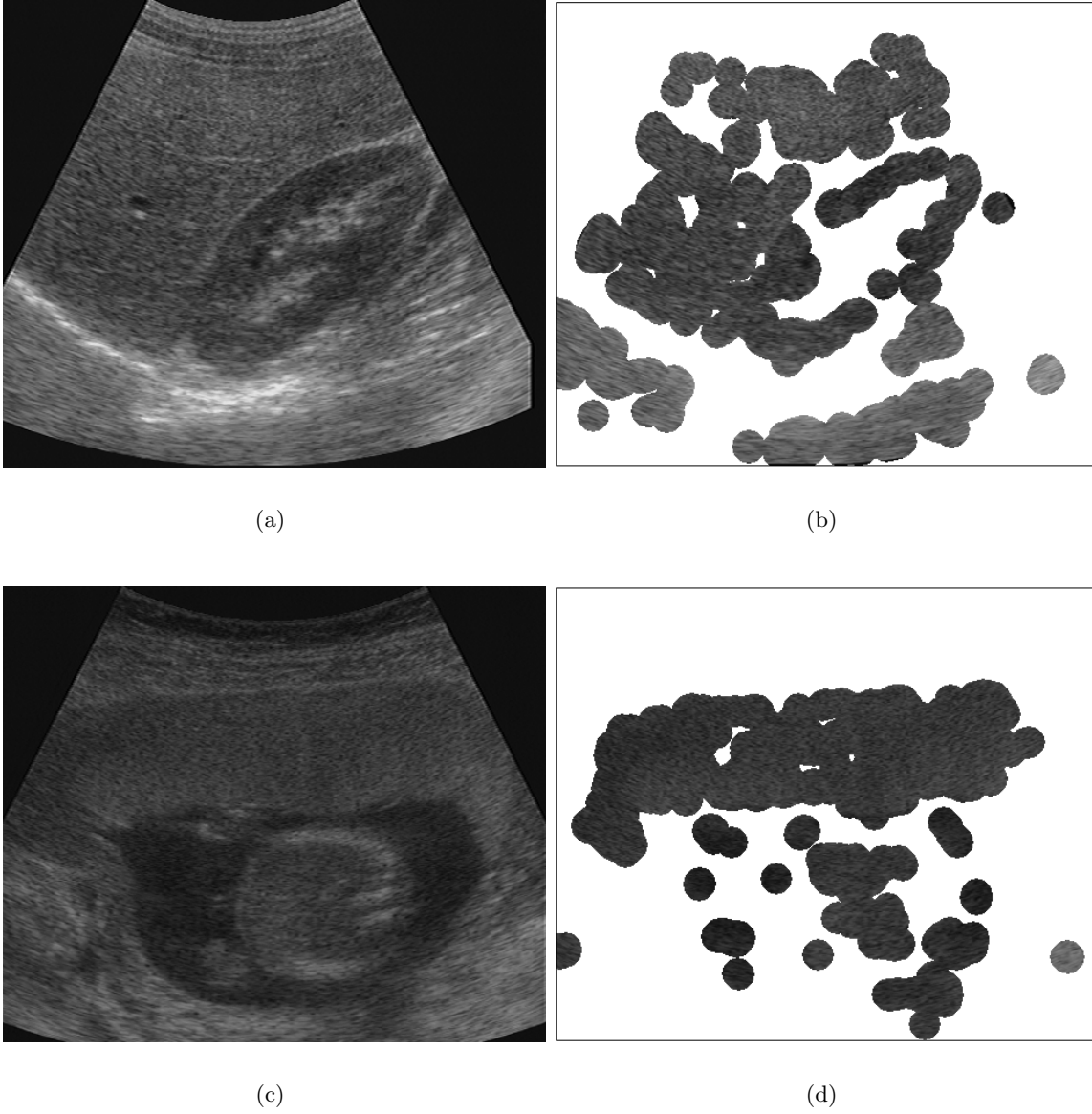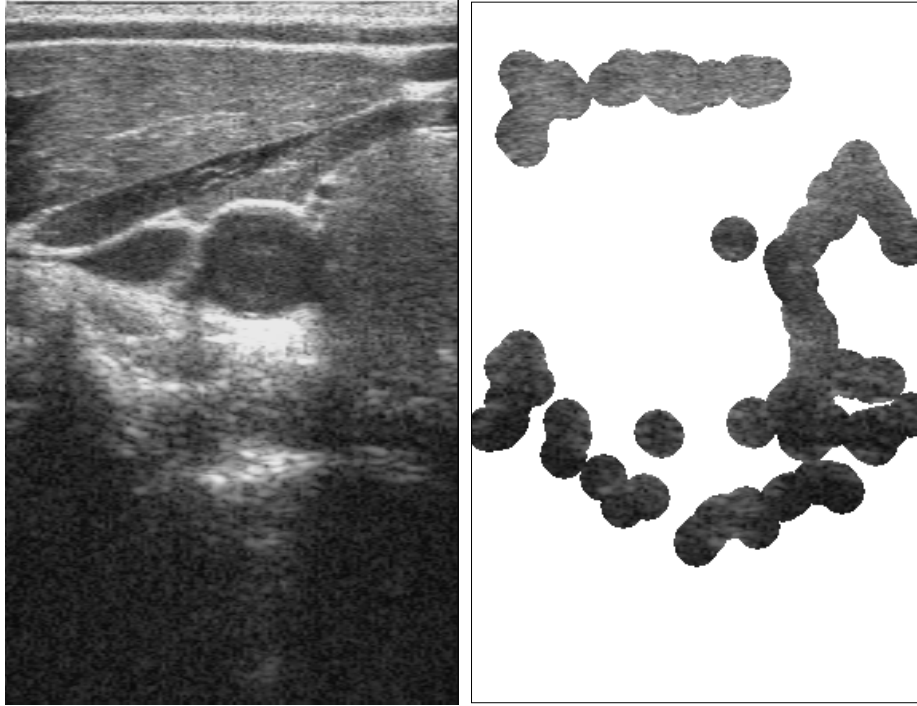(c)   (d)
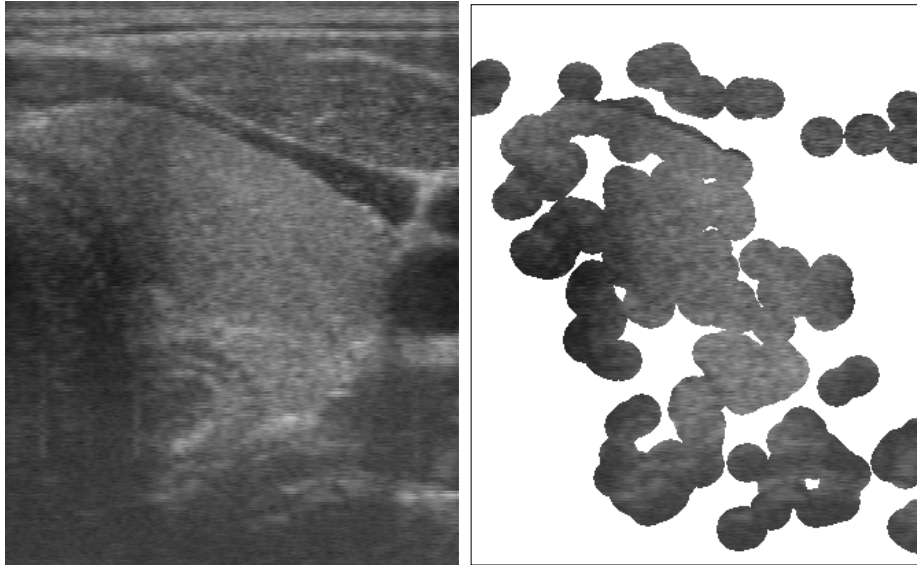
Figure 9: (a) shows an image from an ultrasound scan of a kidney, and (b) shows the regions classified as speckle in this image using the elliptical discriminant function in (R, S) space from Figure 7(b). (c) and (d) show the same thing for a scan of a 16 week fetus in utero. The B-scan used in (a) and (b) of this figure is the same as that shown in (c) and (d) of Figure 5.

Figure 10: (a) shows an image from an ultrasound scan of the carotid artery, and (b) shows the regions classified as speckle in this image using the elliptical discriminant function in (R, S) space from Figure 7(b). (c) and (d) show the same thing for a scan of a thyroid.

fetus is retained but not the coherent scattering near the skin. Figures 10(b) and (d) show speckle in muscle but do not include the dropout at the bottom of the images or the coherent scattering at the tissue interfaces.

6   Conclusions

In real ultrasound images, where coherent scattering may be present, it is not possible to segment speckle based on the mean divided by the standard deviation alone. Another statistic is required to enable both the effective number of scatterers per resolution cell (μ) and the proportion of coherent to diffuse scattering (k) to be inferred. In this report we have studied the use of skewness.

Generalised versions of both the mean over standard deviation (R) and the skewness (S) statistics have been evaluated to determine the best power of the ultrasound echo envelope amplitude values on which to compute them. Surprisingly, our results show that statistics based on powers less than one are not necessarily better for speckle discrimination than statistics based on higher powers.

We have demonstrated that, in simulation, a simple elliptical discriminant function in (R, S) space provides a very efficient way of selecting speckled regions based on thresholds in (k, μ) space. A simplified version of the algorithm has been presented that produces highly plausible results on a variety of approximately decompressed B-scan images.

The work in this report is limited to using only features based on the first order statistics of the data. When we identify speckle manually we look at the appearance of the image and make use of its higher order spectral properties. It must be possible to improve on the speckle detection algorithms presented in this report by incorporating additional information of this sort.

References

[1] V. Dutt. *Statistical analysis of ultrasound echo envelope*. PhD thesis, Mayo Graduate School, August 1995.

[2] V. Dutt and J. F. Greenleaf. Ultrasound echo envelope analysis using a homodyned k distribution signal model. *Ultrasonic Imaging*, 16:265–287, 1994.

[3] V. Dutt and J. F. Greenleaf. Speckle analysis using signal to noise ratios based on fractional order moments. *Ultrasonic Imaging*, 17:251–268, 1995.

[4] E. Jakeman and R. J. A. Tough. Generalized k distribution: a statistical model for weak scattering. *Journal of the Optical Society of America A*, 4(9):1764–1772, September 1987.

[5] F. Ossant, F. Patat, M. Lebertre, M-L. Teriierooiterai, and L. Pourcelot. Effective density estimators based on the k distribution: interest of low and fractional order moments. *Ultrasonic Imaging*, 20:243–259, 1998.

```
coherent

Type of
scatterers        Homodyned k                              Rician

diffuse                   k distribution                   Rayleigh

            few      Number of scatterers        infinite
```
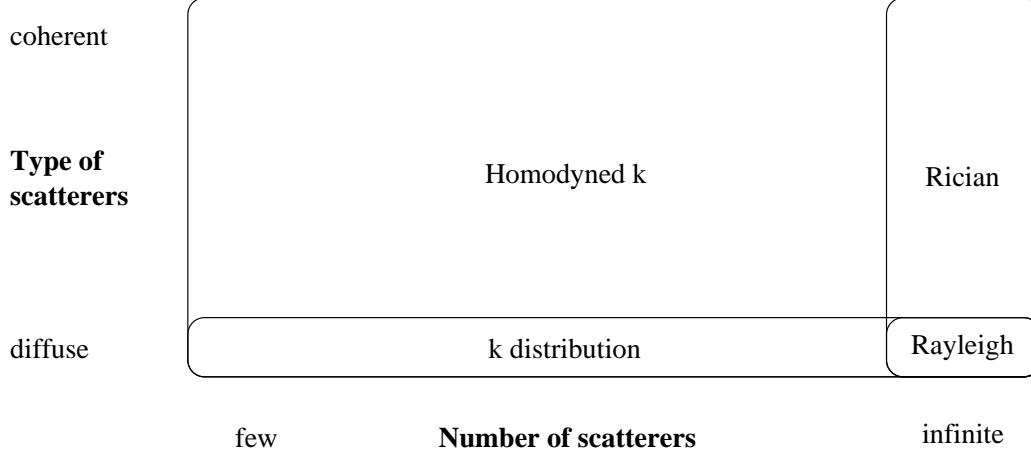
Figure 11: This diagram shows the types of ultrasound images that can be modelled by various distributions. The homodyned k distribution can model images with any number of diffuse scatterers and any proportion of diffuse to coherent amplitude. The k distribution is appropriate for diffuse scattering alone, and the Rician distribution only works when the number of diffuse scatterers tends to infinity. The Rayleigh distribution is applicable only for purely diffuse scattering from many scatterers.

[6] R. W. Prager, A. H. Gee, G. M. Treece, and L. H. Berman. Decompression and speckle detection for ultrasound images using the homodyned k-distribution. Technical Report CUED/F-INFENG/TR.397, Cambridge University Engineering Department, November 2000.

Appendix A: Distributions for modelling speckle

A number of theoretical models are commonly used to model the statistics of the amplitude of the ultrasound echo envelope. Figure 11 shows how they relate to each other. The homodyned k distribution is the most general, with the Rician and k distributions as special cases. The Rayleigh distribution is a special case of both the Rician and k distributions.

The terms in the equations below are defined as follows. s^2 is the coherent backscattered signal energy, $2\sigma^2 = \langle A^2 \rangle$ is the diffuse signal energy and μ is the effective number of scatterers per resolution cell ([3]). $\Gamma(x)$ is the gamma function, $I_n(x)$ is the modified Bessel function of the first kind, $K_n(x)$ is the modified Bessel function of the second kind and $_1F_1$ is the confluent hypergeometric function. The intensity signal I used in the present report is assumed to be distributed as A^2.

Rayleigh distribution

Probability density function.

$$p(A) = \frac{A}{\sigma^2} e^{\frac{-A^2}{2\sigma^2}} \tag{4}$$

Moments.

$$\langle A^v \rangle = \left(2\sigma^2\right)^{\frac{v}{2}} \Gamma \left(1 + \frac{v}{2}\right) \tag{5}$$

Exponential distribution

Probability density function.

$$p(I) = \frac{e^{\frac{-I}{2\sigma^2}}}{2\sigma^2} \tag{6}$$

Moments.

$$\langle I^v \rangle = \left(2\sigma^2\right)^v \Gamma \left(1 + v\right) \tag{7}$$

Rician distribution

Probability density function.

$$p(A) = \frac{A}{\sigma^2} e^{-\frac{A^2 + s^2}{2\sigma^2}} \mathrm{I}_0 \left(\frac{sA}{\sigma^2}\right) \tag{8}$$

Moments.

$$\langle A^v \rangle = \left(2\sigma^2\right)^{\frac{v}{2}} \Gamma \left(1 + \frac{v}{2}\right) {}_1\mathrm{F}_1 \left(-\frac{v}{2}; 1; -\frac{s^2}{2\sigma^2}\right) \tag{9}$$

k distribution

Probability density function.

$$p(A) = \frac{2}{\Gamma(\mu)} \left(\frac{A}{2}\right)^{\mu} \left(\frac{2\mu}{\sigma^2}\right)^{\frac{\mu+1}{2}} \mathrm{K}_{\mu-1} \left(\frac{A\sqrt{2\mu}}{\sigma}\right) \tag{10}$$

Moments.

$$\langle A^v \rangle = \left(\frac{2\sigma^2}{\mu}\right)^{\frac{v}{2}} \Gamma \left(1 + \frac{v}{2}\right) \frac{\Gamma \left(\mu + \frac{v}{2}\right)}{\Gamma \left(\mu\right)} \tag{11}$$

Homodyned k distribution

Probability density function.

$$p_A(A) = \frac{1}{\sigma\Gamma(\mu)} \sqrt{\frac{2\mu A}{\pi s}} \sum_{m=0}^{\infty} \left\{ \frac{\Gamma \left(\frac{1}{2} + m\right)}{m! \, \Gamma \left(\frac{1}{2} - m\right)} \left(\frac{-\sigma^2}{sA\mu}\right)^m \left(\frac{|s - A|\sqrt{\mu}}{\sigma\sqrt{2}}\right)^{\mu+m-\frac{1}{2}} \right.$$

$$\left. \mathrm{K}_{\mu+m-\frac{1}{2}} \left(\frac{|s - A|\sqrt{2\mu}}{\sigma}\right) \right\} \tag{12}$$

Moments.

$$\langle A^v \rangle = \int_0^\infty \left(\frac{2\sigma^2}{\mu}\right)^{\frac{v}{2}} \frac{\Gamma\left(1+\frac{v}{2}\right)}{\Gamma(\mu)} x^{\left(\frac{v}{2}+\mu-1\right)} e^{-x} {}_1\mathrm{F}_1\left(\frac{-v}{2};1;\frac{-\mu s^2}{2\sigma^2 x}\right) dx \tag{13}$$

Moments when $v = 2r$ and r is an integer.

$$\langle A^{2r} \rangle = \left(\frac{2\sigma^2}{\mu}\right)^r \frac{(r!)^2}{\Gamma(\mu)} \sum_{p=0}^r \frac{\Gamma(\mu+r-p)}{(p!)^2 (r-p)!} \left(\frac{s^2\mu}{2\sigma^2}\right)^p \tag{14}$$